

CONSTRAINTS ON HOT METALS IN THE VICINITY OF THE GALAXY

B. McKernan^{1*}, T. Yaqoob^{2,3} and C. S. Reynolds¹

¹*Department of Astronomy, University of Maryland, College Park, MD 20742*

²*Department of Physics and Astronomy, Johns Hopkins University, Baltimore, MD 21218*

³*Laboratory for High Energy Astrophysics, NASA/Goddard Space Flight Center, Greenbelt, MD 20771*

Accepted. Received; in original form

ABSTRACT

We have searched for evidence of soft X-ray absorption by hot metals in the vicinity of the Galaxy in the spectra of a small sample of fifteen type I AGN observed with the high resolution X-ray gratings on board *Chandra*. This is an extension of our previous survey of hot O VII and O VIII absorbing gas in the vicinity of the Galaxy. The strongest absorption signatures within a few hundred km s⁻¹ of their rest-frame energies are most likely due to warm absorbing outflows from the nearest AGN, which are back-lighting the local hot gas. We emphasize that absorption signatures in the spectra of some distant AGN that are kinematically consistent with the recessional velocity of the AGN are most likely to be due to hot local gas. Along the sightline towards PG 1211+143, PDS 456 and MCG-6-30-15 there is a very large absorbing Fe column density which is kinematically consistent with absorption by hot, local Fe. The sightlines to these three AGN pass through the limb of the Northern Polar Spur (NPS), a local bubble formed from several supernovae which, if rich in Fe, may account for a large local Fe column.

We obtain limits on the column density of local, highly ionized N, Ne, Mg, Si along all of the sightlines in our sample. We correlate the column density limits with those of highly ionized O along the same sightlines. Assuming the hot local gas is in collisionally ionized equilibrium, we obtain limits on the temperature and relative abundances of the metals in the hot local gas. Our limits on the ionic column densities in the local hot gas seem to be consistent with those observed in the hot halo gas of edge-on normal spiral galaxies.

Key words: galaxies: active – galaxies: individual – galaxies: Seyfert – techniques: spectroscopic – X-rays: line – emission: accretion – disks :galaxies

1 INTRODUCTION

Present-day structures such as galaxies and clusters of galaxies are believed to have condensed from within partially collapsing filaments of primordial matter. The legacy of the structure formation epoch includes shock-heated filaments as well as structures and these filaments should thread the modern universe. Simulations of structure formation indicate that around half of the baryonic matter at low-redshift lives in such filaments, shock-heated to $\sim 10^{5-7}$ K (see e.g. Cen & Ostriker (1999); Davé *et al.* (2001) and references therein). Although more recent work by Kang *et al.* (2005) suggests that a lower temperature component ($T < 10^5$ K) of the shock-heated filaments may be more significant than previously thought. The ‘warm’ ($\sim 10^{5-6}$ K) com-

ponent of this warm/hot intergalactic medium (WHIGM) has been observed in absorption in the UV band (see e.g. Tripp *et al.* (2000) and references therein). However, much of the WHIGM is expected to be hotter than this, so the high spectral resolution X-ray detectors such as those aboard *Chandra* and *XMM-Newton* are best placed for investigating the ‘hot’ component of the missing baryons.

The clearest X-ray spectral signature of hot gas in the vicinity of our Galaxy consists of absorption features imprinted in spectra of X-ray bright active galactic nuclei (AGN) at $z = 0$ in the observed frame (Hellsten *et al.* 1998; Perna & Loeb 1998). One of the most important new results from the *Chandra* and *XMM-Newton* X-ray telescopes, has been the discovery of hot, low density, highly ionized gas in the vicinity of our Galaxy (at $z = 0$) and possibly beyond (at $z > 0$). X-ray absorption due to local ($z = 0$) hot gas was discovered recently (Nicastró *et al.*

* E-mail: mckernan@astro.umd.edu (BMcK)

2002; Fang *et al.* 2002; Cagnoni 2002; Rasmussen *et al.* 2002; Fang *et al.* 2003; McKernan *et al.* 2003a,b, 2004). Of course, such absorption need not be due to local WHIGM. Absorption by hot gas at $z = 0$ could be due to local Galactic gaseous structures or infalling High Velocity Clouds (see e.g. Sembach *et al.* (2003); Collins, Shull & Giroux (2004) and references therein). Even if there are no known local structures along the sightline to a particular AGN, the location of the absorbing gas is still ambiguous. Around half of all type I AGN exhibit strong absorption in the soft X-ray and UV bands due to partially ionized, optically thin, outflowing, circum-nuclear material known as the ‘warm absorber’ (see e.g. McKernan *et al.* (2005) and references therein). Since the warm absorbers are outflowing, absorption which is actually local to our Galaxy at $z \sim 0$ could be misinterpreted as a warm absorber outflow coinciding with the cosmological recession velocity (cz) of the AGN (see e.g. Fig.3 of McKernan *et al.* (2004)). Confusion with AGN outflow is a worse problem for WHIGM at intermediate redshifts ($z > 0$). The few apparently robust detections of absorbers at redshifts intermediate between our Galaxy and the AGN rest-frame, e.g. Nicastro *et al.* (2005) could be variable (Ravasio *et al.* (2005)) suggestive of an origin in an ionized outflow from the host AGN, rather than WHIGM.

In this paper, we investigate a sample of AGN observed with the high energy transmission gratings (Markert *et al.* 1995) on board *Chandra*. The uniform analysis of the data from these AGN and the results of the analysis, in particular the characterization of the AGN continua and the warm absorption in AGN, have been discussed in detail by (McKernan *et al.* 2005). In McKernan *et al.* (2004) we investigated this sample of AGN spectra for absorption due to local, highly ionized Oxygen. Here we extend that study by searching for absorption in the vicinity of the Galaxy by metals other than Oxygen. Our aim is to further the systematic study of the hot local gas and to begin constraining the temperatures and the relative metal abundances in the hot, local gas.

2 THE SAMPLE AND DATA ANALYSIS

Table 1 lists the AGN sample assembled by McKernan *et al.* (2005). Also listed in Table 1 are the AGN redshifts (from NED¹ using 21cm H I radiation measurements where possible), the AGN Galactic latitude and longitude (also from NED), the Galactic column density and the total exposure times of the spectra. The sample, including selection criteria are discussed in detail in McKernan *et al.* (2005). The *Chandra* data were reprocessed and analyzed according to the methods outlined in (McKernan *et al.* 2005).

Here we extend the study of (McKernan *et al.* 2004) by searching for evidence of absorption by metals less abundant than Oxygen. Table 2 lists the relative solar abundances of the metals relevant for this study. Iron is the next most abundant metal after those listed in Table 2, but there is a forest of Fe L- and M-shell transitions in the soft X-ray

Table 1. The *Chandra* HETGS sample of type I AGN. Columns 2,3 and 4 give the Galactic co-ordinates and the redshift of the source (from NED). Redshift was deduced from observations of the 21cm H I line where possible, since optical estimates of z may be confused by AGN outflow. ^a Galactic column density from Elvis *et al.* (1989), except for Mkn 509 (Murphy *et al.* 1996). The Galactic column density towards F9, NGC 3227, NGC 3516, NGC 3783, NGC 5548, Mkn 766, NGC 7314 and Akn 564 was estimated from interpolations from the measurements of Stark *et al.* (1992). ^b 3C 120 is also classified as a broad-line radio galaxy (NED).

Source	Gal. long. (°)	Gal. lat. (°)	Redshift (z)	Gal. N_H (10^{20}cm^{-2}) ^a
Fairall 9	295.07	-57.83	0.04600	3.0
3C 120 ^b	190.37	-27.40	0.03301	12.30
NGC 3227	216.99	55.45	0.00386	2.15
NGC 3516	133.24	44.40	0.00884	3.05
NGC 3783	287.46	22.95	0.00973	8.50
NGC 4051	148.88	70.09	0.00242	1.31
Mkn 766	190.68	82.27	0.01293	1.80
NGC 4593	297.48	57.40	0.00831	1.97
MCG-6-30-15	313.29	27.68	0.00775	4.06
IC 4329a	317.50	30.92	0.01605	4.55
Mkn 279	115.04	46.86	0.03045	1.64
NGC 5548	31.96	70.50	0.01717	1.70
Mkn 509	35.97	-29.86	0.03440	4.44
NGC 7314	27.14	-59.74	0.00474	1.46
Akn 564	92.14	-25.34	0.02467	6.40

Table 2. Relative solar element abundances relevant for this study. Values are taken from solar photospheric values of Anders & Grevesse (1989). Bahcall *et al.* (2005) suggest that the correct solar abundance of Ne is $[\text{Ne}/\text{H}] = 8.29 \pm 0.05$, values in (brackets) use this value of the solar Ne abundance.

X	$\log(X/O)_\odot$	$\log(X/Ne)_\odot$	$\log(X/Si)_\odot$
O	0.00	0.84(0.64)	1.38
Ne	-0.84(-0.64)	0.00	0.54(0.74)
N	-0.88	-0.04(-0.24)	0.50
Mg	-1.34	-0.50(-0.70)	0.04
Si	-1.38	-0.54(-0.74)	0.00

band (see e.g. Behar *et al.* (2001)). There is therefore considerable ambiguity in Fe absorption line identification due to blending. Furthermore, higher order transitions of more abundant elements can also be mis-identified as Fe transitions. Therefore we limited our search to the strongest absorption transitions in the soft X-ray band in the most abundant highly stripped ions (not O VII and O VIII since we have studied these elsewhere) namely: N VII, Ne IX, Ne X, Mg XI, Mg XII, Si XIII and Si XIV respectively. Table 3 lists the transitions that we investigated in this study, including their rest-frame wavelengths and oscillator strengths.

Once we measured the discrete absorption profiles, we used the extrapolated linear approximation to the curves-of-growth² to obtain a lower limit on the ionic column density

¹ <http://nedwww.ipac.caltech.edu/forms/byname.html>

² The linear part of the curves-of-growth implies that $N_{ion} =$

Table 3. Details of the discrete absorption transitions discussed in this study. f denotes the oscillator strength and λ the wavelength (in \AA) of the respective transitions (values from the Atomic Line List at <http://www.pa.uky.edu/~peter/atomic>).

Ion	Transition	f	$\lambda(\text{\AA})$
N VII	Ly α	0.416	24.7810
Ne IX	(r)1s – 2p	0.724	13.4473
Ne X	Ly α	0.415	12.1339
Mg XI	(r)1s – 2p	0.742	9.1688
Mg XII	Ly α	0.415	8.4210
Si XIII	(r)1s – 2p	0.757	6.6480
Si XIV	Ly α	0.414	6.1822

(N_{ion}), if a *lower limit* on the EW of the absorption feature is available. Such a lower limit on N_{ion} is valid for any value of the velocity width (b) of the absorber. Where no lower limit on the EW exists, absorption is not significant (at 90% confidence). However, in this case, for an assumed b value, we can use the *upper limit* on the EW to get an upper limit on N_{ion} . In such cases, we assumed a velocity width of $b \sim 100 \text{ km s}^{-1}$, since this is roughly the smallest width of a feature that the MEG can resolve although it is considerably larger than the average value of $\langle b \rangle = 40 \pm 13 \text{ km s}^{-1}$ found by Sembach *et al.* (2003) in signatures of local O VI absorption.

3 SPECTRAL FITTING

We used XSPEC v.11.2.0 for spectral fitting to the MEG spectra. All spectral fitting was carried out based on the best-fitting continuum models from (McKernan *et al.* 2005). Spectral fitting was carried out in the 0.5-5 keV energy band, excluding the 2.0-2.5 keV region, which suffers from systematics as large as $\sim 20\%$ in the effective area due to limitations in the calibration of the X-ray telescope³. We analyzed data binned at $\sim 0.02\text{\AA}$, which is approximately the MEG FWHM spectral resolution (0.023\AA). This MEG spectral resolution corresponds to FWHM velocities of ~ 280 and 560 km s^{-1} at observed energies of 0.5 and 1.0 keV respectively. We used the C-statistic (Cash 1976) for finding best-fit model parameters and quote 90% confidence, one-parameter errors.

We proceeded to fit the MEG spectra for the discrete absorption transitions in Table 3 by adding an inverted Gaussian model component to the best-fitting continuum models detailed in McKernan *et al.* (2005). The width of the inverted Gaussian was chosen to be $> 100 \text{ km s}^{-1}$, which is approximately the lower limit of the instrumental velocity resolution. We fixed the redshift of the Gaussian components at $z = 0$ and allowed the rest-energy of the component to vary by $\pm 1200 \text{ km s}^{-1}$ from the rest-frame

energies of the transitions listed in Table 3. The allowed velocity range is identical to that used by Sembach *et al.* (2003) and McKernan *et al.* (2004) in searches for highly ionized Oxygen absorption in the vicinity of the Milky Way.

4 RESULTS

Of the fifteen AGN sightlines in our sample, only the sightlines to NGC 4051 and MCG-6-30-15 exhibit absorption features within $\pm 1200 \text{ km s}^{-1}$ of their rest-frame energy at $z = 0$ at $\geq 99\%$ confidence ($\Delta C \geq 11.3$ for three additional parameters). The sightlines to F9, NGC 4593, NGC 3227 and MCG-6-30-15 exhibit absorption features within $\pm 1200 \text{ km s}^{-1}$ of their rest-frame energy at $z = 0$ at $\geq 90\%$ but $\leq 99\%$ confidence. Of the metals we searched for, only Ne, Mg and Si absorption signatures were detected at $> 90\%$ confidence.

Tables 4 shows the best-fitting model parameters for the strongest detections of Ne IX (r) and Ne X Ly α absorption features. The strongest absorption signatures lie along the sightlines to NGC 4051 and MCG-6-30-15 respectively, where at least one of the Ne absorption features has been detected at $\geq 99\%$ confidence. Table 5 similarly details the best-fit model parameters from a detection of Si XIV Ly α at $> 3\sigma$ significance and a detection of Mg XII Ly α at $> 90\%$ confidence along the sightline to MCG-6-30-15. Listed in Tables 4 and 5 are the equivalent widths (EW) of the absorption features and (in brackets) the improvement in the C-statistic upon addition of the inverted Gaussian model component to the continuum. Also listed in Tables 4 and 5 are the velocity offsets from $z = 0$ of the respective Gaussian centroids and limits on the respective ionic column densities as estimated from a curve-of-growth analysis as outlined above in §2.

Although the features listed in Tables 4 and 5 are statistically significant, the kinematics of most of these features could be consistent with origin in an AGN outflow. The absorption features detected towards NGC 4051 for example, are barely kinematically consistent with an origin in gas at $z = 0$, or indeed with an origin in the same gas (within 90% errors, see Table 4). Nevertheless, at $cz = 725 \text{ km s}^{-1}$, NGC 4051 is very near and with a *Chandra* gratings energy resolution of FWHM $\sim 500 \text{ km s}^{-1}$ at the energy of the Ne IX (r) transition (0.922 keV), it is kinematically difficult to distinguish X-ray absorption intrinsic to the NGC 4051 outflow from X-ray absorption due to hot local gas. Some or most of this hot gas may be associated with the warm absorbing outflow in this AGN.

Along the MCG-6-30-15 sightline, only the Ne IX (r) absorption feature is kinematically consistent with $z = 0$ absorption. The Ne X Ly α absorption feature in Table 4 (at $+615_{-235}^{+295} \text{ km s}^{-1}$), coincides kinematically with the Si XIV Ly α and Mg XII Ly α absorption features in Table 5 (at $\sim +615$ and $\sim +530 \text{ km s}^{-1}$), but these features are not kinematically consistent with an origin in hot local gas at $z = 0$. Thus, we conclude that the Ne X Ly α , Si XIV Ly α and Mg XII Ly α features along the sightline to MCG-6-30-15 originate in a warm absorber outflowing from the AGN at -1710 km s^{-1} rather than hot local gas (see also McKernan *et al.* (2005)). Therefore, in order to study the hot *local* Ne X Ly α along the sightline to MCG-6-30-15,

$1.13 \times 10^{17} EW/f\lambda^2$ where N_{ion} is the ionic column density (cm^{-2}), EW is the equivalent width of the absorption feature (in m\AA), f is the oscillator strength of the transition and λ is in \AA .

³ <http://asc.harvard.edu/udocs/docs/POG/MPOG/node13.html>

Table 4. Results of spectral fitting for absorption due to hot Ne within ± 1200 km s $^{-1}$ from transition rest-energies at $z = 0$. Of the four absorption features listed here, only one is likely to be mostly due to hot local gas (see text for discussion). Columns 2 and 3 show the best-fit EW for Ne IX (r) and Ne X Ly α respectively and (in brackets) the improvement in the fit-statistic upon the addition of the inverted Gaussian model component to the continuum. Columns 4 and 5 show the ionic column densities of Ne IX and Ne X respectively as estimated from a curve-of-growth analysis (see text for details). Column 6 shows the velocity centroid offset from $z=0$ (LSR) of the Ne IX (r) and Ne X Ly α features respectively. (log) Column densities are rounded to the nearest 0.05.

Sightline	EW(Ne IX (r)) (eV)(ΔC)	EW(Ne X Ly α) (eV)(ΔC)	$N_{\text{Ne IX}}$ (cm $^{-2}$)	$N_{\text{Ne X}}$ (cm $^{-2}$)	$v(\text{Ne IX})$ (km s $^{-1}$)	$v(\text{Ne X})$ (km s $^{-1}$)
NGC 4051	$2.64^{+0.79}_{-0.95}$ (17.6)	$1.14^{+0.54}_{-0.66}$ (7.2)	16.60 ± 0.15	$16.45^{+0.20}_{-0.40}$	$+420^{+520}_{-450}$	-175^{+205}_{-295}
MCG-6-30-15	$0.89^{+0.38}_{-0.50}$ (8.4)	$1.03^{+0.59}_{-0.48}$ (11.3)	$16.05^{+0.20}_{-0.25}$	$16.40^{+0.25}_{-0.35}$	-65^{+260}_{-165}	615^{+295}_{-235}

we searched for upper limits on absorption due to Ne X Ly α by adding a narrow inverted Gaussian to the spectrum at -65 km s $^{-1}$ from $z = 0$ rest-frame energy (to compare with the corresponding Ne IX (r) absorption). We obtained upper limits on absorption due to Mg XII Ly α and Si XIV Ly α similarly by adding a narrow inverted Gaussian at the $z = 0$ rest-frame energy of the transition. Likewise, for NGC 4051, we obtained upper limits on absorption due to Ne IX and Ne X by adding narrow inverted Gaussians at the rest-frame energy of the respective absorption transitions at $z = 0$.

Fig. 1 is a multipanel plot showing velocity profiles of the Ne IX (r) and Ne X Ly α absorption features along the sightlines to NGC 4051 and MCG-6-30-15. The profiles are centered on the Ne IX (r) transition energy (0.9220 keV) and the Ne X Ly α transition energy (1.0218 keV) in the LSR respectively (both energies are denoted by vertical dashed lines at 0 km s $^{-1}$). The vertical dotted line in Fig. 1(a,b) at $+110$ km s $^{-1}$ denotes the weighted mean offset velocity of the O VII and O VIII absorption along this sightline detected by McKernan *et al.* (2004). The vertical dash-dot line in Fig. 1(a,b) at $+725$ km s $^{-1}$ denotes the recessional velocity (cz) of NGC 4051. Superposed on the data is the best-fit inverted Gaussian absorption line model (from Table 4) and continuum (horizontal solid line).

Of the less significant absorption features detected (at $\geq 90\%$ confidence but $< 99\%$ confidence), those along the sightlines towards F9 and NGC 4593 are kinematically coincident with their rest-energies at $z = 0$ and are therefore likely to correspond to hot local gas. A Si XIV Ly α feature detected at an offset velocity of -525^{+450}_{-600} km s $^{-1}$ along the sightline towards NGC 3227 is more likely to kinematically correspond to an outflow at ~ 1700 km s $^{-1}$ from the AGN ($cz = 1160$ km s $^{-1}$) than absorption due to hot, local gas. We obtained upper limits on absorption due to Si XIV along this sightline by fitting a narrow inverted Gaussian to the continuum at the rest-energy of Si XIV Ly α at $z = 0$.

4.1 Local, hot gas versus AGN outflow?

NGC 4051 and MCG-6-30-15 are two of the closest AGN in our sample, at recessional velocities of $cz = 726$ km s $^{-1}$ and $cz = 2325$ km s $^{-1}$ respectively. Since the spectra of Type I AGN typically exhibit hot gas outflowing at several hundred km s $^{-1}$, the proximity of these two AGN, raises the important issue of confusion between absorption due to hot gas at $z = 0$ and that due to a warm absorber

Table 5. As for Table 4, except for Mg XII Ly α and Si XIV Ly α along the sightline to MCG-6-30-15. These features are kinematically consistent with the Ne X Ly α feature along this sightline in Table 4 above. Therefore these absorption features are most likely due to a hot absorbing outflow from MCG-6-30-15 at ~ -1710 km s $^{-1}$ (see text).

Transition	EW (eV)(ΔC)	N (cm $^{-2}$)	vel (km s $^{-1}$)
Mg XII Ly α	$1.56^{+1.10}_{-0.98}$ (8.2)	$16.55^{+0.20}_{-0.40}$	$+530^{+450}_{-550}$
Si XIV Ly α	$2.96^{+0.98}_{-1.01}$ (23.1)	$16.60^{+0.15}_{-0.20}$	$+615^{+255}_{-285}$

(see also the discussion in McKernan *et al.* (2004)). The proximity of NGC 4051 and MCG-6-30-15 (and NGC 3227) and the limited gratings spectral resolution makes it difficult to distinguish X-ray absorption features along these sightlines due to hot local gas from those due to warm absorbing outflows. On the other hand, the more distant the AGN, the more likely it is that absorption signatures at offset velocities very close to their $z = 0$ rest-frame energy are due to hot, local gas. The relation in Figure 3 of McKernan *et al.* (2004) shows this effect quite dramatically. Thus, outflows previously thought to be associated with more distant AGN, e.g. PG 1211+143 (Pounds *et al.* 2003) and PDS 456 (Reeves *et al.* 2003) are kinematically much more likely to correspond to hot, local gas. We note that the surprisingly high Fe column densities towards both of these AGN might be accounted for by the intersection of both of these sightlines with the limb of the local Northern Polar Spur (NPS) structure. A third sightline through the NPS, towards MCG-6-30-15 also exhibits strong absorption due to a large column of highly ionized Fe that is kinematically consistent with a local origin (Young *et al.* 2005). The NPS is a local feature believed to correspond to the superposition of several supernovae and is clearly seen in X-ray emission maps (see e.g. Snowden *et al.* (1997)) and in maps of polarization towards nearby stars (Mathewson & Ford 1970; Heiles & Jenkins 1976; Axon & Ellis 1976). An alternative hypothesis is that the NPS may actually be a much larger feature subtended at the Galactic center Sofue (2000); Bland-Hawthorn & Cohen (2003), although we shall not consider this hypothesis further here. If the progenitor supernovae of the NPS were rich in pure Fe, this could account for the anomalous column of Fe along these sightlines. We intend to investigate this possibility in future work.

4.2 Column densities of hot local metals

Table 6 lists the limits on the ionic column densities for all the ions from spectral fitting. Most of the results in Table 6 are upper limits, indicating that discrete absorption features due to local gas are not detected at $> 90\%$ confidence in most cases. None of the sightlines exhibited absorption due to local N at $> 90\%$ confidence. The spectra of three AGN, namely NGC 3227, NGC 3516 and NGC 7314, were too heavily absorbed at ≤ 0.8 keV even to obtain meaningful limits on N VII absorption. We found that assuming different values of the velocity width (e.g. $b \sim 50$ or ~ 200 km s^{-1}), led to small changes in estimates of N_{ion} in Table 6, $\log(\Delta N_{ion}) < 0.2$ for $b = 50$ km s^{-1} and $\log(\Delta N_{ion}) < 0.1$ for $b = 200$ km s^{-1} respectively using the linear part of the curves-of-growth.

Sembach *et al.* (2003) and McKernan *et al.* (2004) associate local, highly ionized O absorption with known local structures such as the Magellanic Stream (MS), Complex C and Extreme Positive North (EPn), as well as a diffuse Local Group (LG) and (potentially) the warm/hot IGM. Several of the sightlines in Table 6 can be identified with these structures: one (F9) with the MS, three (NGC 4593, NGC 4051, NGC 3227) are identified with EPn and one (MCG-6-30-15) which we associate with the NPS. In the southern Galactic hemisphere, the sightline to Akn 564 passes through the Magellanic Stream extension (MSE), but this may also be LG (Sembach *et al.* 2003).

Sembach *et al.* (2003) conclude that most of the high velocity ($v \sim 100$ -400 km s^{-1}) O VI gas in the vicinity of the galaxy is created by collisional ionization. Furthermore, gas in the low redshift IGM is far more likely to be collisionally ionized than photoionized (Heckman *et al.* 2002). Therefore, if we assume that the hot gas in the vicinity of the Galaxy is in collisional ionization equilibrium (CIE), and that the absorption signatures discussed here and in McKernan *et al.* (2004) are due to the same gas, it is possible to establish temperature constraints on the gas, whether it is local to our Galaxy or low redshift WHIGM. Sutherland & Dopita (1993) calculate $N_{Ne IX}/N_{Ne X}$ and $N_{Si XIII}/N_{Si XIV}$ for gas in CIE, so where there are statistically significant lower limits on an ionic column along a given sightline, we can constrain the temperature of local gas along that sightline with some confidence. However, from searching for seven absorption transitions along each of fifteen different sightlines through the hot, local gas, there are only three *lower* limits on ionic column densities. The corresponding temperature limits (assuming CIE) using the $N_{Ne IX}/N_{Ne X}$ ratio are: $T < 10^{6.75}$ K towards MCG-6-30-15, $T < 10^{6.70}$ K towards NGC 4593 and $T > 10^{6.35}$ K towards F9. The sightline to F9 provides a *lower* limit on the temperature because we detect Ne X Ly α and not Ne IX (r).

5 COMPARISON WITH SIGNATURES OF OXYGEN ABSORPTION

McKernan *et al.* (2004) showed that seven of the fifteen sightlines in our sample exhibit discrete absorption features due to local O VII and O VIII. Sembach *et al.* (2003) found local O VI ($\lambda 1031.926$ Å) absorption along 59 of 102 sight-

lines towards UV bright AGN/QSOs at high Galactic latitudes ($|b| \geq 30^\circ$). Several of the 59 sightlines coincide with sightlines in our sample (F9, NGC 5448, Mkn 509, Akn 564), of which three (F9, Mkn 509, Akn 564) show significant O VI absorption. In Figure 2, we show the sightlines to the fifteen AGN in our sample in Hammer-Aitoff projection. Crosses indicate non-detection of *any* highly ionized local gas (Ne, Mg, Si and O) along the sightline. Triangles indicate detection (at $> 90\%$ confidence) of highly ionized local gas (Ne or Si) with no corresponding highly ionized O. Diamonds indicate the presence of local, highly ionized O along the sightline, but non-detection of local, highly ionized Ne, Mg and Si. Filled-in circles indicate sightlines along which highly ionized Ne or Si has been detected (at $> 90\%$ confidence) *and* which show absorption due to local, highly ionized O.

Of the three sightlines which exhibit absorption by local, highly ionized Ne at $> 90\%$ confidence (listed in Table 6), two sightlines (F9 and NGC 4593) also exhibit absorption by O VII and/or O VIII at $> 90\%$ confidence (McKernan *et al.* 2004). The sightline towards F9 also exhibits O VI absorption (Sembach *et al.* 2003). The sightlines to MCG-6-30-15 does not exhibit absorption due to highly ionized Oxygen. In McKernan *et al.* (2004) we constrained the temperature in local gas from limits on $N_{OVIII,VII,VI}$ and an assumption of CIE. Towards F9, we found $10^{5.75} < T < 10^{6.35}$ K. This is marginally inconsistent with our estimate of $T > 10^{6.35}$ K using $N(Ne IX, Ne X)$ in §4 above. However, the condition that $T < 10^{6.35}$ K along this sightline is derived assuming a b-parameter of precisely 100 km s^{-1} using N_{OVIII} in a curve-of-growth analysis. A choice of a slightly larger b-parameter (which would be allowed by the data) would yield a temperature upper limits compatible with that derived using $N(Ne IX, Ne X)$. The combined results using $N(O VI, O VII, O VIII, Ne IX \& Ne X)$ along the sightline to F9, suggests that the temperature in the local hot gas in the MS is close to $T \sim 10^{6.35}$ K and that there is some velocity broadening of the hot gas along this sightline. The temperature of the gas along the sightlines to NGC 5448 and Akn 564 was also constrained by McKernan *et al.* (2004) to be $T > 10^{6.2}$ K and $T < 10^{6.1}$ K respectively. However, the absence of significant absorption along the sightlines to NGC 5548 and Akn 564 in this study (see Table 6), means that we cannot provide additional constraints on the temperature of gas along these sightlines.

6 POSSIBLE CONSTRAINTS ON METALLICITIES IN HOT LOCAL GAS

The temperature ranges derived from the ratios of column densities in §4 above and by (Sembach *et al.* 2003) and (McKernan *et al.* 2004) suggest that we can assume that most of the O, Ne, Mg and Si in the hot gas in the vicinity of the Galaxy is in H-like and He-like ions. If we assume that the gas is in CIE, then for a range of temperatures, such as those discussed here, the fraction in H-like or He-like ions is much larger than in other ionic states (Sutherland & Dopita 1993) (e.g. in the case of Oxygen ions, $O VIII / O IX \gg 1$, $O VII / O VI \gg 1$). Thus, in a simple approximation, the largest upper (or lower) limit on the column density of the He-like or H-like ions of a particular element is ap-

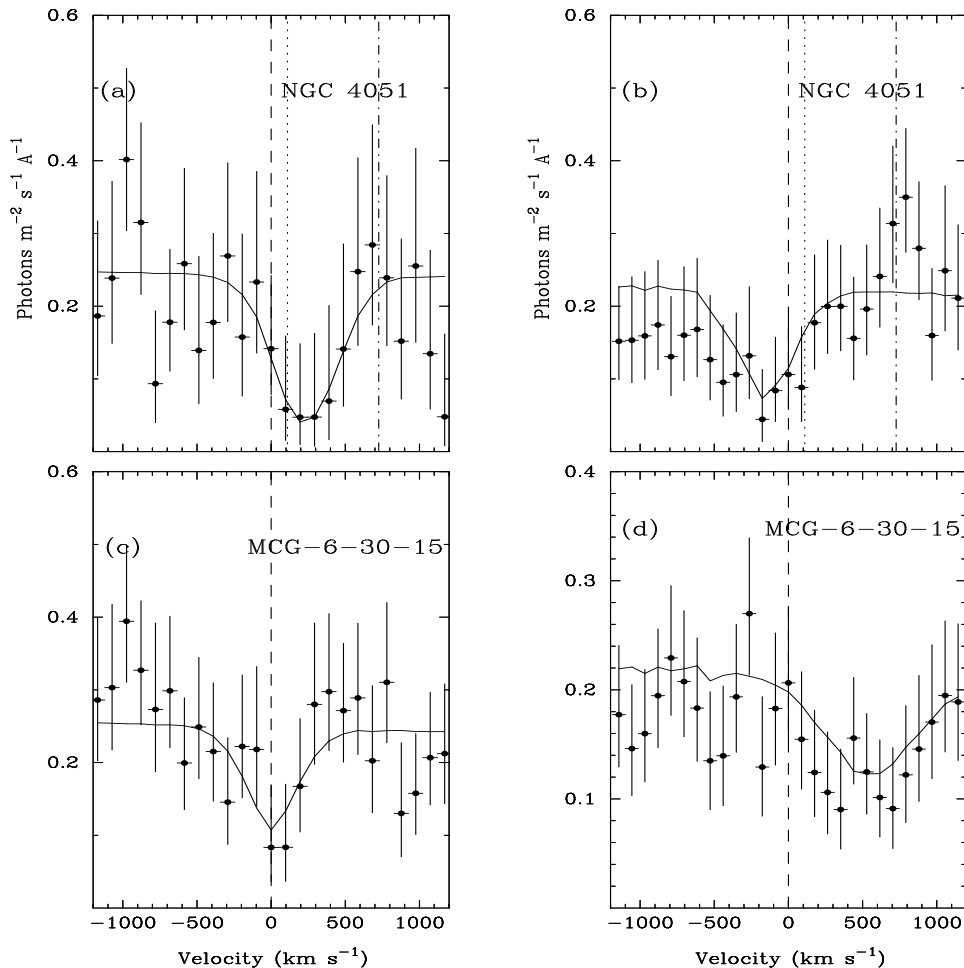


Figure 1. Velocity profiles from combined ± 1 order *Chandra* MEG data from the AGN in Table 4, centered on the LSR Ne IX (r) transition energy (0.9220 keV) in the left column panels and on the Ne X Ly α transition energy (1.0218 keV) in the right column panels (dashed lines). A positive velocity indicates a redshift relative to these energies. The velocity spectra data have been uniformly binned at 0.3eV which is approximately the limit of the MEG resolution (0.3eV is the FWHM resolution at ~ 0.4 keV or about 1/5th the FWHM at the Ne IX (r) transition energy). Vertical dotted lines in panels (a) and (b) indicate the weighted mean offset velocity $cz = +110 \pm 115$ km s $^{-1}$ of absorption due to O VII and O VIII (from McKernan *et al.* (2004)). Vertical dash-dot lines indicate the rest-frame of NGC 4051 ($cz=726$ km s $^{-1}$). The rest frame of MCG-6-30-15 ($cz=2325$ km s $^{-1}$) lies outside the ± 1200 km s $^{-1}$ range of these panels. Superposed is the best-fit inverted Gaussian absorption line model (from Table 4) and continuum (horizontal solid line). Of the four profiles shown here, only the Ne IX (r) feature towards MCG-6-30-15 is likely to be entirely due to hot, local gas (see text). The features towards NGC 4051 are most likely due in large part to a warm absorbing outflow from this AGN.

proximately the upper (lower) bound on the amount of the element present.

Therefore, given a lower limit to the column density $N(X)$ of an element X, using this simple approximation, we can use upper limits on the column density $N(Y)$ of element Y to obtain a lower limit on $N(X)/N(Y)$ along a sightline. Limits on relative metal abundances in the hot local gas, allow us to compare the results with solar relative abundances (see Table 2) and thereby establish limits on the composition of the hot gas. The relative depletion or enrichment of certain metals can provide clues to the environment, formation and evolution of the hot gas in local structures and the hot IGM. Note that it is not possible to obtain reliable upper limits on the ratio $N(X)/N(Y)$, since an upper limit on $N(X)$ is potentially much more inaccurate than a lower limit (a firm lower bound on the column), due to the possibility

Table 7. The (log) abundances of elements relative to Oxygen in the hot gas in the vicinity of the Galaxy, assuming CIE. Values in (brackets) correspond to a solar Ne abundance from (Bahcall *et al.* 2005).

Sightline	[O/Ne]	[O/N]	[O/Mg]	[O/Si]
\odot	0.84(0.64)	0.90	1.29	1.38
F9	> -0.90	> 0.80	> -0.50	> -1.20
3C 120	> -1.22	> -2.86	> -1.03	> -0.47
NGC 3783	> 0.04	> 0.06	> 0.08	> 0.95
NGC 4051	> -0.35	> -0.24	> -0.22	> -1.30
NGC 5548	> -0.87	> -0.46	> -0.49	> -0.42
Mkn 509	> -0.93	> -1.16	> -0.85	> -0.77

of additional columns of more or less ionized gas than those considered here.

Table 6. Results of spectral fitting for hot gas at $z = 0$ as discussed in text. Columns 2-8 show the logarithm of the ionic column densities of N VII, Ne IX, Ne X, Mg XI, Mg XII, Si XIII and Si XIV respectively as estimated from a curve-of-growth analysis as described in the text. (log) Column densities are rounded to the nearest 0.05. Lower limits on ionic column densities are valid for all values of b . Upper limits are valid for an assumed velocity width of 100 km s^{-1} (unless specified otherwise) which is approximately the lower bound on the instrumental resolution. A choice of $b = 100 \text{ km s}^{-1}$ is larger than the values inferred by S03 for local O VI absorption features. ^a The soft X-ray spectrum is too absorbed to obtain limits.

Sightline	(log) $N_{\text{N VII}}$ (cm^{-2})	$N_{\text{Ne IX}}$ (cm^{-2})	$N_{\text{Ne X}}$ (cm^{-2})	$N_{\text{Mg XI}}$ (cm^{-2})	$N_{\text{Mg XII}}$ (cm^{-2})	$N_{\text{Si XIII}}$ (cm^{-2})	$N_{\text{Si XIV}}$ (cm^{-2})
F9	< 15.30	< 17.00	$16.35^{+0.25}_{-0.35}$	< 16.15	< 16.60	< 17.30	< 16.10
3C 120	< 18.60	< 16.90	< 15.85	< 15.70	< 16.75	< 16.65	< 16.20
NGC 3227	^a	< 16.40	< 16.70	< 18.95	< 16.90	< 17.75	< 17.10
NGC 3516	^a	< 16.70	< 16.95	< 16.15	< 16.30	< 17.35	< 16.70
NGC 3783	< 15.80	< 15.80	< 14.95	< 15.75	< 15.20	< 14.75	< 14.90
NGC 4051	< 16.70	< 15.90	< 16.80	< 16.65	< 16.60	< 17.75	< 16.70
Mkn 766	< 16.95	< 15.85	< 16.10	< 16.40	< 16.35	< 17.30	< 16.25
NGC 4593	< 16.65	$16.05^{+0.25}_{-0.80}$	< 16.10	< 16.20	< 16.15	< 16.35	< 16.45
MCG-6-30-15	< 16.65	$16.05^{+0.20}_{-0.25}$	< 16.25	< 18.15	< 16.55	< 15.95	< 16.50
IC 4329A	< 17.70	< 16.50	< 15.95	< 15.50	< 16.35	< 15.90	< 16.25
Mkn 279	< 16.10	< 16.50	< 16.45	< 16.80	< 16.50	< 16.05	< 16.45
NGC 5548	< 16.40	< 16.10	< 16.80	< 16.40	< 16.35	< 16.20	< 16.35
Mkn 509	< 16.45	< 16.20	< 15.80	< 16.10	< 16.10	< 16.05	< 15.80
NGC 7314	^a	< 17.05	< 16.80	< 15.90	< 16.50	< 17.55	< 16.45
Akn 564	< 16.20	< 15.85	< 15.85	< 16.20	< 16.35	< 16.75	< 16.20

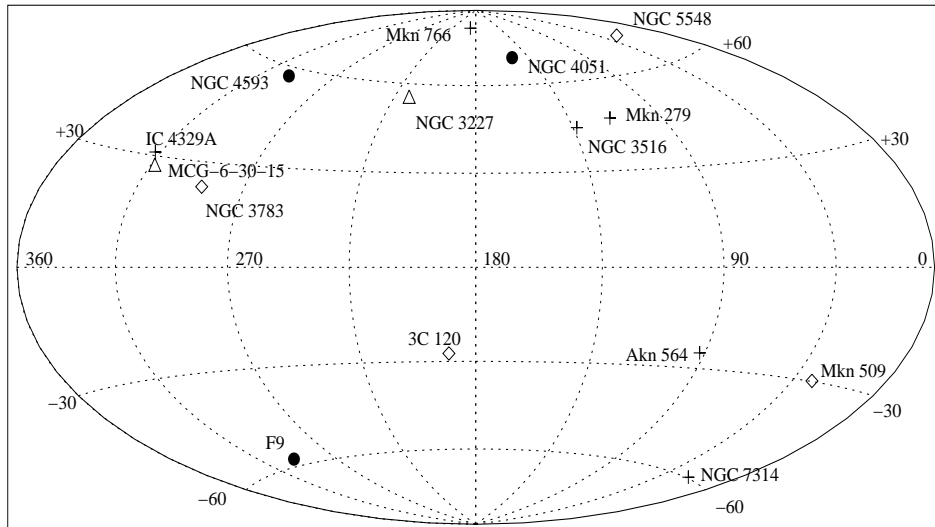


Figure 2. All-sky Hammer-Aitoff projection of the sightlines to the 15 AGN in this study. In this projection, the Galactic anticenter is at the center of the figure and Galactic longitude increases to the left. Crosses indicate nondetection of local, highly ionized Ne, Mg, Si or O along the sightline (measurements of O from McKernan *et al.* (2004)). Diamonds indicate non-detection of local, highly ionized Ne or Si, but detection of highly ionized O along the sightline. Triangles indicate detection of local, highly ionized Ne or Si along the sightlines at $> 90\%$ confidence, but no corresponding absorption due to local, highly ionized O. Filled-in circles denote detection of local, highly ionized Ne or Si along the sightlines at $> 90\%$ confidence *plus* corresponding local, highly ionized O absorption.

Table 8. The (log) abundance of Ne relative to O, N, Mg and Si in the hot gas in the vicinity of the Galaxy. We assumed CIE in calculating these ratios. Values in (brackets) correspond to a solar Ne abundance from (Bahcall *et al.* 2005). ^a There is no meaningful upper limit on N(O) for the the sightline to F9, since $\log N(\text{O VII}) > 16.1$ (possible saturation) and $\log N(\text{O VIII}) < 16.6$ (McKernan *et al.* 2004).

Sightline	[Ne/O]	[Ne/N]	[Ne/Mg]	[Ne/Si]
☉	-0.84(-0.64)	0.04(0.24)	0.50(0.70)	0.54(0.74)
F9	^a	> 0.70	> -0.60	> -1.30
NGC 4593	> -1.99	> -1.41	> -0.96	> -1.19
MCG-6-30-15	> -0.85	> -0.60	> -0.15	> -0.60

Tables 7 and 8 list constraints on the metal abundances relative to O and Ne respectively, in the hot gas in the vicinity of our Galaxy. Clearly the lower limits on the relative abundances in the local, hot gas are in general too small to be interesting, with a few exceptions. In Table 7, the lower limit on [O/N] along the sightline to F9 is close to the solar value, while the other ratios are one or two orders of magnitude lower, which may suggest a relative underabundance of N in the MS. Also in Table 7, the lower limit on [O/Si] along the sightline to NGC 3783 is close to the solar ratio, while the other ratios are significantly lower, which may be hinting at a relative underabundance of Si along this sightline. In Table 8, [Ne/N] along the sightline to F9 *exceeds* the solar value by ~ 3.9 , and [Ne/Si] along the sightline to MCG -6-30-15 is roughly solar. The other Ne ratios are one or two orders of magnitude below their solar values. This again suggests an underabundance of N in the hot gas in the MS.

7 CONCLUSIONS

Half of the baryonic matter in the local universe seems to be missing. The search for the hottest component of the missing matter has only been possible with the latest generation of high spectral resolution X-ray telescopes. Hot gas in the vicinity of the Galaxy may be due to local WHIGM or it may reside either in a hot Galactic halo or locally in a thick disk and has only recently begun to be studied in the X-ray band. We assembled a small sample of type I AGN observed with the high resolution X-ray gratings on board *Chandra* and we have applied a uniform analysis to detect soft X-ray absorption by hot gas in the vicinity of our Galaxy. This study is an extension of our previous study of O VII and O VIII absorption by hot local gas (McKernan *et al.* 2004).

Three of the fifteen sightlines in our sample (towards F9, NGC 4593 and MCG-6-30-15 respectively) exhibit Ne IX (r) or Ne X Ly α absorption due to hot, local gas at $\geq 90\%$ confidence. We identify these absorption features with the hot phase of local structures. Such local structures are either in the disk of the Galaxy (e.g. the Local Bubble or superbubbles such as the NPS) or lie above the disk in HVCs or other structures, such as a Galactic halo. Hot gas in a thick disk is expected to have low offset velocity from $z = 0$ (typically $\leq 100 \text{ km s}^{-1}$) and hot gas above the disk in HVCs or in a Galactic halo is expected to have a higher offset velocity from $z = 0$ (typically $100 - 400 \text{ km s}^{-1}$). The

sightlines to the AGN in our sample lie well away from the Galactic plane ($b \geq 30^\circ$) and *Chandra* does not possess the velocity resolution to distinguish between kinematic signatures of a thick disk or Galactic halo. Therefore we cannot tell whether absorption is local to the disk, or further out in a halo, where there are no known local structures along a sightline. Absorption studies in the UV band with *FUSE* indicate that there is a thick Galactic disk of O VI, with a scale height of $\sim 2.3 \text{ kpc}$, as well as a patchy overdensity of O VI in the northern Galactic hemisphere from $b \sim 45^\circ$ to 90° due to the Local Bubble and superbubbles (including the NPS) (Savage *et al.* 2003). X-ray spectral studies of Galactic X-ray binaries confirm that there is a hot, thick disk with scale height of $\sim 1 - 2 \text{ kpc}$ associated with our Galaxy (see e.g. Futamoto *et al.* (2004); Yao & Wang (2005)). The column densities inferred from Futamoto *et al.* (2004); Yao & Wang (2005) are consistent with the limits inferred here, so it may be that most or all of the hot gas locally is associated with a Galactic 'thick disk' of hot gas, with enrichment along particular sightlines in the northern Galactic hemisphere due to local superbubbles such as the NPS.

There can be considerable ambiguity in distinguishing local hot absorbing gas and hot absorbing outflows from AGN, especially with the limited spectral resolution of the *Chandra* gratings. This is particularly true of some of the AGN in the present study. Two sightlines in our study (towards MCG-6-30-15 and NGC 4051 respectively) exhibit absorption features within $\pm 1200 \text{ km s}^{-1}$ of their rest-energies at $z = 0$ at confidence levels $> 99\%$. However, the kinematics of the absorption signatures suggest that these features are most likely due to absorption in hot gas outflowing from the respective background AGN. Nevertheless, the more distant the AGN, the more likely that absorption signatures in the AGN spectrum which kinematically coincide with the AGN recession velocity are due to hot, local gas. This is demonstrated by the relation in Fig. 3 of (McKernan *et al.* 2004). Two of the AGN in Fig. 3 of (McKernan *et al.* 2004), namely PG 1211+143 and PDS 456, also exhibit absorption due to a very large local column of Fe, which is surprising. We point out that absorption by the local NPS bubble, if Fe-enriched, could account for the very large column density of Fe along the sightline to these AGN, and towards MCG-6-30-15 as well. Thus, hot gas in the disk of the Galaxy may account for much of the $z = 0$ absorption in the soft X-ray spectra of several AGN.

We assumed collisionally ionized equilibrium (CIE) to use limits on ionic column densities to derive limits on the temperatures in the hot, local gas. We find that in the southern Galactic hemisphere, the sightline to F9 through the MS yields $T > 10^{6.35} \text{ K}$, which is marginally consistent with our temperature limits from $N(\text{O VII})/N(\text{O VIII})$ (McKernan *et al.* 2004). Likewise, in the northern Galactic hemisphere we find temperature limits of $T < 10^{6.75} \text{ K}$ towards MCG-6-30-15 and $T < 10^{6.70} \text{ K}$ towards NGC 4593. For a range of temperatures, such as those discussed here, derived limits on the H- and He-like ion column densities allow us to establish constraints on the relative abundances of N, Ne, Mg and Si (as well as O from McKernan *et al.* (2004)) along the sightlines in our sample. In general, we found lower limits on the relative abundances of the metals that are one or two orders of magnitude below the corre-

sponding solar values (see Tables 7 and 8). However, we do find evidence for a relative *underabundance* of N in the hot gas in the MS along the sightline towards F9.

The question of whether the hot gas detected in the vicinity of the Galaxy is in part (or at all) associated with the missing matter remains as yet unanswered. The environment of the Galaxy is complex, consisting of satellite galaxies (Magellanic Clouds), tidal trails (the Magellanic Stream), infalling HVCs and outflows from supernovae in the Galaxy. Standard theories of structure formation in the universe suggest that our Local Group (our Galaxy and M31) should have formed from a low density filament of gas, the heated remnants of which should persist today. The local filament should be metal-enriched by outflows from structures that formed within it. However, the upper limits on column densities that we derive here and in McKernan *et al.* (2004) seem to be consistent with estimates of column densities from studies of Galactic halos in edge-on normal spiral galaxies (Strickland *et al.* 2004). Thus, our first systematic (but hardly comprehensive) look at the hot, X-ray absorbing component of gas in the vicinity of our Galaxy suggests that our Galaxy is embedded in a hot halo or hot thick disk.

ACKNOWLEDGMENTS

We gratefully acknowledge support from NSF grant AST0205990 (BM) and NASA grant AR4-5009X issued by CXC operated by SAO under NASA contract NAS8-39073 (TY). We made use of the HEASARC on-line data archive services, supported by NASA/GSFC and also of the NASA/IPAC Extragalactic Database (NED), operated by the Jet Propulsion Laboratory, CalTech, under contract with NASA. Thanks to the *Chandra* instrument and operations teams for making the observations possible. Thanks to M. Coleman Miller, David Strickland and Andy Fabian for useful discussions and thanks to Ken Sembach for bringing to our attention the uncertainty in the solar Ne abundance. Thanks to the anonymous referee for their comments which helped improve this paper.

REFERENCES

- Anders, E., & Grevesse, N. 1989, *Geochim. Cosmochim. Acta*, 53, 197
- Axon, D. J., & Ellis, R. S. 1976, *MNRAS*, 177, 499
- Bahcall, J. N., Basu, S. & Serenelli, A. M. 2005, *astro-ph/0502563*
- Behar, E., Sako, M. & Kahn, S. M. 2001, *ApJ*, 570, 165
- Bland-Hawthorn, J., & Cohen, M., 2003, *ApJ*, 582, 246
- Cagnoni, I., 2002, *astro-ph/0212070*
- Cash, W., 1976, *A&AS*, 52, 307
- Cen, R., & Ostriker, J. P., 1999, *ApJ*, 514, 1
- Collins, J. A., Shull, J. M. & Giroux, M. L., 2004, *ApJ*, 605, 216
- Davé, R., *et al.* 2001, *ApJ*, 552, 473
- Elvis, M., Wilkes, B. J., Lockman, F. J. 1989, *AJ*, 97, 777
- Fang, T., Marshall, H. L., Lee, J. C., Davis, D. S., Canizares, C. R., 2002, *ApJ*, 572, L127
- Fang, T., Sembach, K. R., Canizares, C. R., 2003, *ApJ*, 586, L49
- Futamato, K., Mitsuda, K., Takei, Y., Fujimoto, R. & Yamasaki, N. Y., 2004, *ApJ*, 605, 793
- Hellsten, U., Gnedin, N. Y. & Miralde-Escudé, J. M. 1998, *ApJ*, 509, 56
- Heckman, T. M., Norman, C., Strickland, D. K. & Sembach, K. R. 2002, *ApJ*, 577, 691
- Heiles, C., & Jenkins, E. B. 1976, *A&A*, 46, 333
- Kang, H., Ryu, D., Cen, R. & Song, D. 2005, *ApJ*, 620, 21
- Markert, T. H., Canizares, C. R., Dewey, D., McGuirk, M., Pak, C., & Shattenburg, M. L. 1995, *Proc. SPIE*, 2280, 168
- Mathewson, D. S., & Ford, V. L. 1970, *MNRAS*, 74, 139
- McKernan, B., Yaqoob, T., George, I. M., Turner, T. J., 2003a, *ApJ*, 593, 142
- McKernan, B., Yaqoob, T., Mushotzky, R., George, I.M., Turner, T. J. 2003b, *ApJ*, 598, L83
- McKernan, B., Yaqoob, T., Reynolds, C. S. 2004, *ApJ*, 617, 232.
- McKernan, B., Yaqoob, T., Reynolds, C. S. 2005, *MNRAS*, submitted.
- Murphy, E. M., Lockman, F. J., Laor, A., Elvis, M. 1996, *ApJS*, 105, 369
- Nicastro, F. *et al.* 2002, *ApJ*, 573, 157
- Nicastro, F. *et al.* 2005, *Nature*, 433, 495
- Perna, R. & Loeb, A. 1998, *ApJ*, 503, L135
- Pounds, K. A., Reeves, J. N., King, A. R., Page, K. L., O'Brien, P. T. & Turner, M. J. L. 2003, *MNRAS*, 345, 705
- Rasmussen, A., Kahn, S. M., Paerels, F., 2002, in 'The IGM/Galaxy connection-the distribution of Baryons at z=0', Colorado (Kluwer Academic Publishing) (*astro-ph/0301183*)
- Ravasio, M., Tagliaferri, G., Pollock, A. M. T., Ghisellini, G., Tavecchio, F., 2005, *A&A* (in press), *astro-ph/0502567*
- Reeves, J. N., O'Brien, P. T. & Ward, M. J. 2003, *ApJ*, 593, L65
- Savage, B. D. *et al.* 2003, *ApJS*, 146 ,125
- Sembach, K. R. *et al.* 2003, *ApJS*, 146 ,165
- Snowden, S. L. *et al.* 1997, *ApJS*, 485, 125
- Sofue, Y., 2000, *ApJ*, 540, 224
- Strickland, D. K., Heckman, T. M., Colbert, E. J. M., Hoopes, C. G., Weaver, K.A. 2004, *ApJS*, 151, 193
- Sutherland, R. S., Dopita, M. A. 1993, *ApJS*, 88, 253
- Tripp, T. M., Savage, B. D. & Jenkins, E. B. 2000, *ApJ*, 534, L1
- Yao, Y., Wang, Q. D., 2005, *ApJ*, 624, 751
- Young, A. J., Reynolds, C. S. *et al.* 2005, *ApJ* submitted

This paper has been typeset from a \TeX / \LaTeX file prepared by the author.